Friction effects on quasi-steady dam-break wave propagation on horizontal beds

Nielsen, Peter; Xu, Beibei; Wüthrich, Davide; Zhang, Shaotong

DOI
10.1017/jfm.2022.182

Publication date
2022

Document Version
Final published version

Published in
Journal of Fluid Mechanics

J. Fluid Mech. (2022), *vol*. 939, A21, doi:10.1017/jfm.2022.182

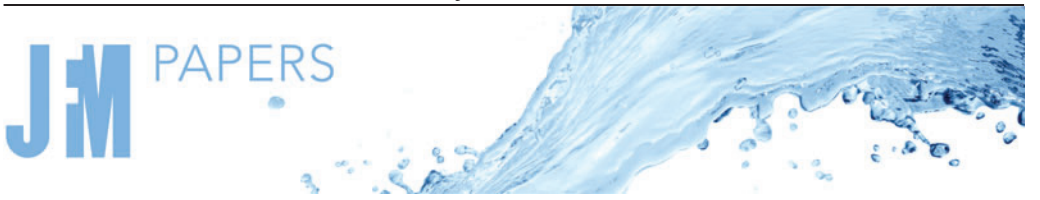

Friction effects on quasi-steady dam-break wave propagation on horizontal beds

Peter Nielsen[1],†, **Beibei Xu**[2], **Davide Wüthrich**[1,3] **and Shaotong Zhang**[4]

[1]The University of Queensland, Brisbane, QLD 4067, Australia

[2]College of Harbour, Coastal and Offshore Engineering, Hohai University, Nanjing 210098, China

[3]Delft University of Technology, Delft 2600, The Netherlands

[4]Key Laboratory of Submarine Geosciences and Prospecting Techniques (Ministry of Education), Ocean University of China, Qingdao 266100, China

(Received 8 November 2021; revised 26 January 2022; accepted 24 February 2022)

The propagation of dam-break waves on different rough beds was observed to be quasi-steady in the range $11.3 < x/h_{dam} < 18.8$, where x is measured from the dam position. These quasi-steady propagation speeds converge with the steady ideal fluids model of Stoker (*Water Waves*, 1957, Interscience) when the tailwater depth h_2 becomes greater than $\sim 0.5k_s$, in the range $0.001 < k_s/h_{dam} < 0.2$, where k_s is the roughness and h_{dam} the depth behind the dam. Hence, this convergence encourages the use of Stoker's steady, ideal fluid solution to develop more general models, including friction effects due to bed roughness and/or viscosity. The new experimental data support a MacLaurin series for the celerity c, in analogy with the series in terms of $\sqrt[4]{h_2/h_{dam}}$, derived for Stoker's model, h_2 being the tailwater depth. Compared with the retarding effect of the tailwater, 1 mm of roughness is found to be equivalent to ∼13 mm of tailwater, and 1 μm of viscous length ($\nu/\sqrt{gh_{dam}}$, where ν is the kinematic viscosity and g the acceleration due to gravity) is equivalent to ∼1700 μm of tailwater. While the MacLaurin series quantifies the similar effects of small roughness and small tailwater depths acting separately, the new data illustrate for the first time the complex interplay between tailwater and roughness on 'wet beds' with many details yet to be investigated. In particular, it was shown that a small amount of tailwater on a rough bed acts as a lubricant, so that $c(h_2, h_{dam}, k_s)$ is an increasing function of h_2 for $h_2 < 0.5k_s$.

Key words: wave breaking, hydraulics

† Email address for correspondence: p.nielsen@uq.edu.au

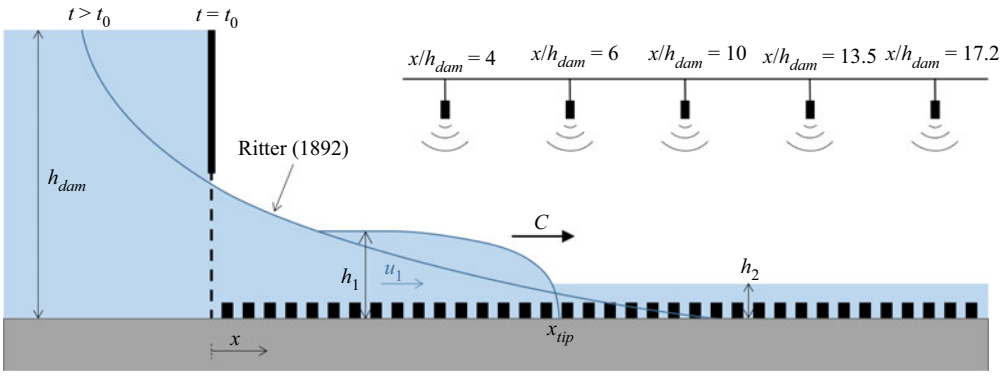

Figure 1. Definition sketch of the main variables and experimental set-up.

1. Introduction

The progressing fronts of wave run-ups, tsunamis and dam-break waves are capable of catastrophic flooding and severe structural damage, as well as reshaping of the inundated geomorphology through vigorous sediment entrainment and transport. They do therefore deserve, and have received, much attention from fluid mechanic and hydraulic researchers. Understanding and predictive capabilities are, however, still limited because of the unsteady and non-uniform aspects of the flow near the tip, which needs a different boundary layer description from steady, uniform river flows and periodically oscillating wave boundary layers. The present study is fairly narrowly focused on the effects of viscosity and bed roughness on quasi-steady propagation speeds on horizontal beds. But it is the ambition that these results will facilitate studies on the flow structure and sediment transport in tsunamis, wave run-ups and dam-break waves on natural, sloping beds.

Historically, the method of characteristics was used to find a solution of the dam-break problem for an ideal fluid in an infinite, prismatic, horizontal channel (Ritter 1892). This explicit analytical solution provides the theoretical framework and scaling for interpreting experiments, even if these experiments involve real, viscous fluids in less idealised flume geometries. In Ritter's scenario (figure 1) the tip is chisel sharp and propagates with steady speed $2\sqrt{gh_{dam}}$ (where g is the acceleration due to gravity and h_{dam} the depth behind the dam), but it is unsteady in the sense that the depth at any given distance x behind the tip varies with time. In agreement with the general expectation, experiments by Schoklitsch (1917) showed that the sharp tip of Ritter's ideal fluids solution is unrealistic due to the neglect of friction, caused by a combination of viscosity and bed roughness.

Dressler (1952, 1954) and Whitham (1955) therefore developed dam-break models with bull-nose tips for the propagation on dry beds and these models have subsequently been expanded or simplified by several authors, e.g. Chanson (2009). In these models, the tip speed decreases with time, which is in agreement with observations of the initial stages, i.e. $x_{tip}/h_{dam} < 10$, where x_{tip} is the distance of the tip from the dam position, i.e. $x = 0$. The behaviour of the tip in the initial stages is highly complex and not necessarily well described by these hydrostatic models, as demonstrated by Stansby, Chegini & Barnes (1998). Also, the form of the analytical solutions of Dressler (1952) and Whitham (1955) has not led to investigation of the possible existence of a (quasi-) steady asymptotic state for large t or x_{tip}.

A parallel stream of models was started by Stoker (1957), showing that a quasi-steady bore develops after some distance, when an ideal fluid dam-break wave progresses into

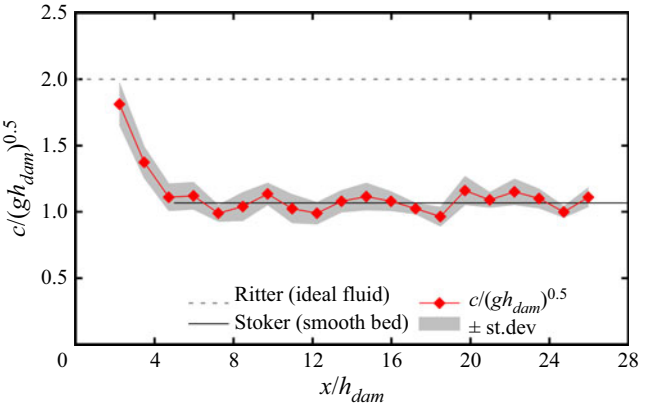

Figure 2. Observed tip propagation speeds for a selected test with $h_{dam} = 0.4\,\text{m}$, $k_s = 2.4\,\text{mm}$ and $h_2 = 0.018\,\text{m}$. Results clearly show the quasi-steady nature of the propagating bore. Details of the experiments are given in § 4.

resting tailwater on a horizontal bed. Like the friction considered by Dressler (1952) and Whitham (1955), the opposing momentum of the tailwater in the frame of reference of the moving bore has the effect of thickening the tip and slowing down its progression compared with Ritter's dry bed, ideal fluid solution. Stoker's treatment of the bore as a shock (with unspecified length or shape) simplifies matters compared with the pre-existing friction-affected models.

The present study uses Stoker's quasi-steady paradigm to investigate the effects of roughness, tailwater depth and viscosity, as well as the interplay between roughness and tailwater depth, on the bore propagation. Our experiments indicate that a shock (or bore) generally forms, and becomes quasi-steady, also for rough beds, with or without a tailwater depth (h_2) (figure 1). A typical example of this quasi-steady behaviour reached by the bore is shown in figure 2. The length or time scale required by the tip's celerity c to reach a quasi-steady state (i.e. $x/h_{dam} = 4$ in figure 2) becomes shorter with increased resistance from tailwater depth and/or bed roughness, as perhaps indicated by the general form of Dressler's and Whitham's solutions $c = 2\sqrt{gh_{dam}}[1 - \sqrt[3]{R}t + \cdots]$, where R is a measure of the frictional resistance.

The oscillations of the propagation speed in figure 2, herein with amplitude of $\sim$10 % of the ideal fluid speed $2\sqrt{gh_{dam}}$, depends on h_2/h_{dam} and k_s/h_{dam} via the complicated initial wave conditions discussed by Stansby *et al.* (1998). The quasi-steady approach is found to give instructive comparisons with Stoker's steady shock model at least for $10 < x_{tip}/h_{dam} < 17.5$. That is, such comparisons, including both wet and dry beds with a variety of relative roughness (k_s) ($0.025 < k_s/h_{dam} < 0.2$), show that the observed quasi-steady propagation speeds converge to Stoker's smooth bed, ideal fluids values (c_{ideal}) when the effects of increasing tailwater depth eventually dominate over the roughness and/or viscous effects.

The paper is structured as follows: § 2 reviews Stoker's model and § 3 derives the MacLaurin series for the tip celerity in terms of $\sqrt[4]{h_2/h_{dam}}$, which clarifies the behaviour for $h_2/h_{dam} \to 0$, which is difficult to reproduce with experiments. Section 4 describes the new dam-break experiments. Section 5 compares the retarding effects of the roughness of dry rough beds, respectively of viscosity, with that of ideal fluid tailwater depth. Section 6 is discussion on challenges for further research, followed by the main conclusions.

2. Stoker steady bore propagation model

The following is a restatement of the Stoker (1957) model (§ 10.8) for a steady, ideal fluid bore on a horizontal bed, recast in order to facilitate derivation of an explicit expression for the propagation speed. For an ideal fluid on a wet (i.e. $h_2 > 0$), smooth, horizontal bed, the momentum equation together with conservation of volume gives the bore propagation speed

$$c_{ideal} = \sqrt{g\frac{h_1 + h_2}{2} \times \frac{h_1}{h_2}}, \tag{2.1}$$

where c_{ideal} is the bore front celerity and h_1 the flow depth behind the bore front (see e.g. Lecture 51 of the lectures by Feynman, Leighton & Sands (1964) and definition sketch in figure 1). Equating the bore flow rate to a driving unit flow rate q gives

$$q = (h_1 - h_2) \times c_{ideal} = (h_1 - h_2) \times \sqrt{g\frac{h_1 + h_2}{2} \times \frac{h_1}{h_2}}, \tag{2.2}$$

which can be solved very effectively for h_1 by simple iteration, if rewritten as

$$h_1 = \sqrt[4]{\frac{2h_2q^2}{g\left(1 + \dfrac{h_2}{h_1}\right)\left(1 - \dfrac{h_2}{h_1}\right)^2}} \tag{2.3}$$

while the limit for $h_2/h_1 \to 0$ is

$$h_1 \simeq \sqrt[4]{\frac{2h_2q^2}{g}}, \quad \text{for } h_2 \to 0, \tag{2.4}$$

showing an asymptotic behaviour of h_1 for vanishing tailwater depths, in line with the theory of Ritter (1892) for smooth beds (figure 1). While q remains implicitly dependent on h_1 and h_2, following Stoker (1957) or Stansby *et al.* (1998) for a dam-break wave in an infinitely long, prismatic channel, q can be expressed in terms of the dam height h_{dam} and the constant depth h_1 behind the bore as $q = 2h_1\sqrt{g}[\sqrt{h_{dam}} - \sqrt{h_1}]$, that introduced into (2.3) leads to

$$h_1 = \sqrt[4]{\frac{2h_2 4h_1^2 g[\sqrt{h_{dam}} - \sqrt{h_1}]^2}{g\left(1 + \dfrac{h_2}{h_1}\right)\left(1 - \dfrac{h_2}{h_1}\right)^2}}, \tag{2.5}$$

which becomes

$$h_1 = \frac{\sqrt{8h_2}[\sqrt{h_{dam}} - \sqrt{h_1}]}{\sqrt{1 + \dfrac{h_2}{h_1}\left(1 - \dfrac{h_2}{h_1}\right)}} \tag{2.6}$$

and with the limit

$$h_1 \simeq \sqrt{8h_2h_{dam}}, \quad \text{for } \frac{h_2}{h_1}, \frac{h_1}{h_{dam}} \to 0, \tag{2.7}$$

as previously stated by Pritchard & Hogg (2002). Solving (2.6) by iteration gives the curve for h_1 and the bore height $H = h_1 - h_2$, shown in figure 3. Inserting the value of h_1 into

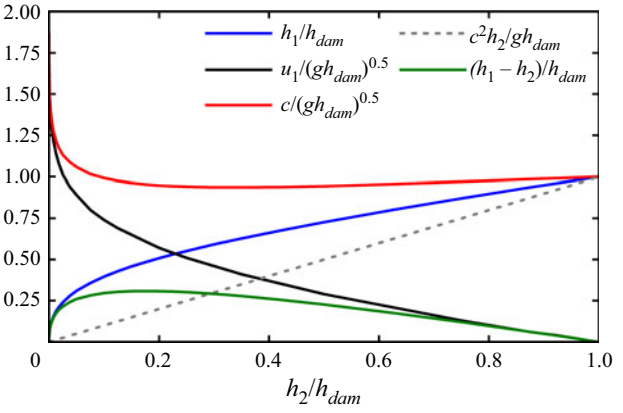

Figure 3. Dimensionless, steady depth behind the bore h_1/h_{dam}, bore height $H/h_{dam} = (h_1 - h_2)/h_{dam}$, celerity $c/(gh_{dam})^{0.5}$, depth-averaged velocity behind the bore $u_1/(gh_{dam})^{0.5}$ and c^2h_2/gh_{dam} according to Stoker (1957).

(2.1) gives c_{ideal} and the depth-averaged velocity behind the bore $u_1 = (1 - h_2/h_1)c_{ideal}$, whose behaviour is also shown in figure 3.

Inserting Stoker's bore depth (2.6) into the celerity expression (2.1) gives the propagation speed for ideal fluid on a smooth horizontal bed

$$c_{ideal} = \sqrt{g\left(\frac{\dfrac{\sqrt{8h_2}[\sqrt{h_{dam}} - \sqrt{h_1}]}{\sqrt{1 + \dfrac{h_2}{h_1}\left(1 - \dfrac{h_2}{h_1}\right)}} + h_2}{2} \cdot \frac{\dfrac{\sqrt{8h_2}[\sqrt{h_{dam}} - \sqrt{h_1}]}{\sqrt{1 + \dfrac{h_2}{h_1}\left(1 - \dfrac{h_2}{h_1}\right)}}}{h_2}\right)} \tag{2.8}$$

that can be rewritten as

$$c_{ideal} = 2\sqrt{gh_{dam}\left(\frac{1 - \sqrt{\dfrac{h_1}{h_{dam}}}}{\sqrt{1 + \dfrac{h_2}{h_1} \cdot \left(1 - \dfrac{h_2}{h_1}\right)}} + \sqrt{\frac{h_2}{8h_{dam}}}\right)\left(\frac{1 - \sqrt{\dfrac{h_1}{h_{dam}}}}{\sqrt{1 + \dfrac{h_2}{h_1} \cdot \left(1 - \dfrac{h_2}{h_1}\right)}}\right)}, \tag{2.9}$$

which, since $h_1/h_{dam}, h_2/h_1 \to 0$ for $h_2 \to 0$ matches the Ritter value on a dry bed

$$c_{ideal} \to 2\sqrt{gh_{dam}}. \tag{2.10}$$

A numerical evaluation of the results gives the curve in figure 3, including a local minimum propagation speed of $\sim 0.94\sqrt{gh_{dam}}$ occurring for $h_2/h_{dam} \approx 0.35$.

3. MacLaurin series for Stoker's bore front celerity

Using the limit expression in (2.6), i.e. $h_1/h_{dam} \to \sqrt{8(h_2/h_{dam})}$ for $h_2 \to 0$, it can be inferred that the second term in (2.10) is $2^{7/4}(h_2/h_{dam})^{1/4}$, as previously shown by

Pritchard & Hogg (2002). Further investigations lead to

$$\frac{c_{ideal}}{\sqrt{gh_{dam}}} = 2 - 2^{7/4}\left(\frac{h_2}{h_{dam}}\right)^{1/4} + 5\times 2^{-1/2}\left(\frac{h_2}{h_{dam}}\right)^{1/2} - 5\times 2^{-7/4}\left(\frac{h_2}{h_{dam}}\right)^{3/4} + 2^{-3}\frac{h_2}{h_{dam}} - \cdots, \tag{3.1}$$

or approximately

$$\frac{c_{ideal}}{\sqrt{gh_{dam}}} = 2 - 3.36\left(\frac{h_2}{h_{dam}}\right)^{1/4} + 3.54\left(\frac{h_2}{h_{dam}}\right)^{1/2} - 1.49\left(\frac{h_2}{h_{dam}}\right)^{3/4} + 0.12\frac{h_2}{h_{dam}} - \ldots. \tag{3.2}$$

The behaviour of this MacLaurin series is 'erratic' for $h_2/h_{dam} \to 1$, but (3.2) is within 1 % of the numerical solution for the practically relevant range $0 < h_2/h_{dam} < 1$.

4. New experiments

For the present investigation, new dam-break tests were carried out in a 13 m long, 0.5 m wide and 0.45 m deep flume at the University of Queensland (Australia). A vertical PVC gate across the whole channel width was used to release the impounded volume, estimated to approximately 0.6 m^3. The gate was operated manually and the opening time was sufficiently short to respect the criterion by Lauber & Hager (1998), i.e. $0.2\,\text{s} < \sqrt{2h_{dam}/g} \approx 0.3\,\text{s}$. For all tests the initial depth behind the dam was $h_{dam} = 0.40\,\text{m} \pm 0.01\,\text{m}$ and the flume bed was horizontal. In order to delay the dam-depletion effects on the bore propagation, a discharge of $Q \approx 0.18\,\text{m}^3\,\text{s}^{-1}$ was continuously supplied after the gate opening. Nine dry bed tests with rubber mats and $h_2 = 0$ were performed on different days, leading to an average wave front celerity $c = 1.687\,\text{m}\,\text{s}^{-1} \pm 0.046\,\text{m}\,\text{s}^{-1}$, thus confirming the accuracy and repeatability of the set-up. The tailwater depth h_2 was measured from the flat PVC base under the roughness elements. In addition to the smooth PVC bed, four different roughnesses were used: two rubber mats with different thicknesses (26 and 16 mm), artificial plastic grass (∼5mm) and roof gutter mesh glued onto the PVC (table 1). The friction parameters were determined by fitting the universal law of the wall for steady uniform flows

$$u(z) = \frac{u_f}{\kappa}\ln\frac{z-\Delta z}{z_0} \approx \frac{u_f}{\kappa}\ln\frac{z-\Delta z}{\dfrac{k_s}{30} + 0.11\dfrac{\nu}{u_f}}, \tag{4.1}$$

where κ is the von Kármán constant, z the vertical direction and the zero intercepts z_0 from the curve fitting are interpreted as $k_s/30$ under fully rough, turbulent conditions. This methodology was applied to all the rough beds in this study as well as $0.11\nu/u_f$ for smooth turbulent conditions (PVC bed). The friction velocity was determined as $u_f = \sqrt{S_S g(z_{surface} - \Delta z)}$, S_S being the surface slope, $z_{surface}$ the elevation of the free surface and g the gravitational acceleration. Results are listed in table 1 and the measured velocity profiles, scaled according to the parameters in table 1, are compared with the universal log law (4.1) in figure 4.

https://doi.org/10.1017/jfm.2022.182 Published online by Cambridge University Press

Description	z_0 (mm)	k_s (mm)	Δz (mm)	κ (—)	Flow depth (mm)	Surface slope S_S (—)	u_f (m s^{-1})	q (m^2 s^{-1})
Rubber mat (26 mm)	28	84	12.5	0.40	275	0.0092	0.154	0.324
Rubber mat (16 mm)	20	60	2.0	0.40	265	0.0109	0.168	0.360
Flat PVC	0.0012	smooth	0	0.48	219	0.0031	0.081	0.372
Artificial grass (5 mm)	0.60	18	3.5	0.38	284	0.0042	0.108	0.351
Gutter mesh (5 × 5 × 1 mm)	0.08	2.4	0	0.48	248	0.0068	0.128	0.400

Table 1. Friction parameters of the tested configurations and flow conditions.

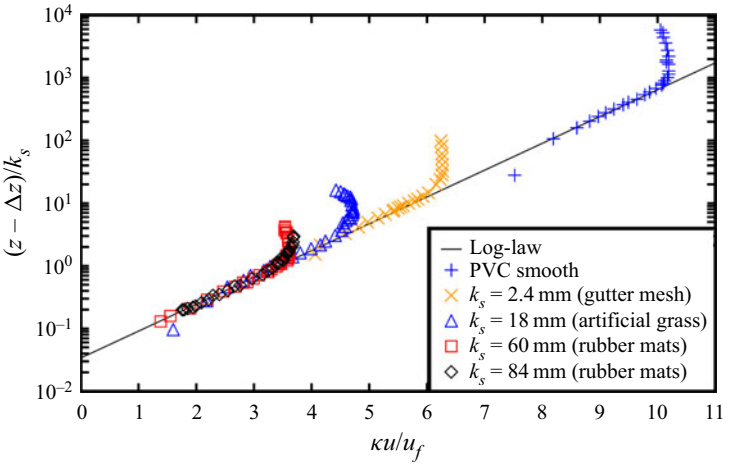

Figure 4. Universal log-law fits for determining the friction parameters of the present experiments.

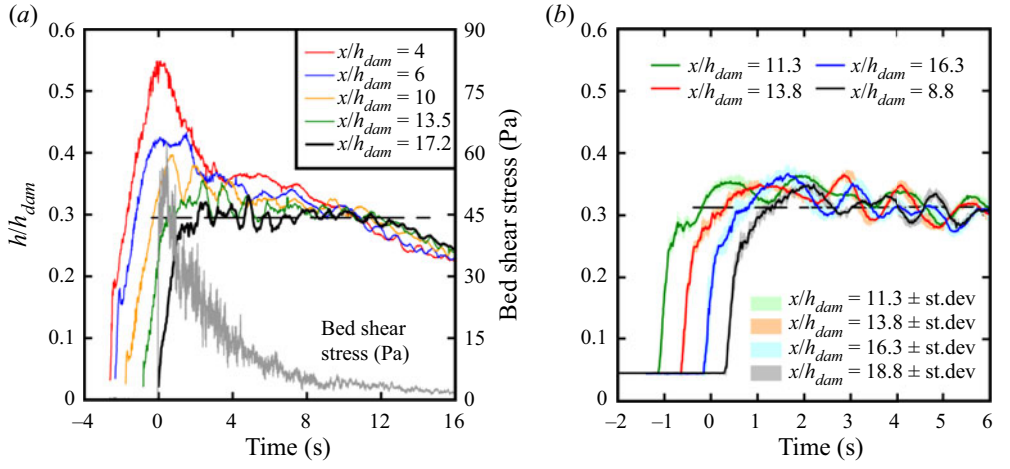

Figure 5. (*a*) Surface elevations and bed shear stress measured on a dry bed with $k_s = 60$ mm and $h_{dam} = 0.4$ m. (*b*) Surface elevations on a wet bed with $k_s = 2.4$ mm, $h_2 = 0.018$ m and $h_{dam} = 0.4$ m (same as figure 2). Time $T = 0$ s represents the bore's arrival at $x/h_{dam} = 17.2$. Dashed line represents the experimental bore's depth behind the front, h_1.

Surface elevations were measured with acoustic displacement sensors (Microsonic^{TM} mic+25/IU/TC, Germany). The celerity c was computed as the ratio of the distance between two sensors and the bore's travel time. An example of surface elevations at various locations from the dam is shown in figure 5 with simultaneous bed shear stress measurements at $x/h_{dam} = 17.2$. The bed shear stresses were measured with the shear plate developed by Barnes & Baldock (2019), dynamically calibrated via step response tests indicating a natural frequency (in water) of 25 Hz (Xu *et al.* 2021). Results for a dry bed surge in figure 5(*a*) indicate that the water depth remains quasi-constant for a relatively long time (8–9 s) at $x/h_{dam} = 17.2$, compared with the time scales of bed shear stress rise and decay at the same position. In addition, data for a wet bed bore in figure 5(*b*) show similar time series of the water depths at $11.3 < x/h_{dam} < 18.8$, indicating that the moving bore has reached a good degree of uniformity in the x-direction, which is in line

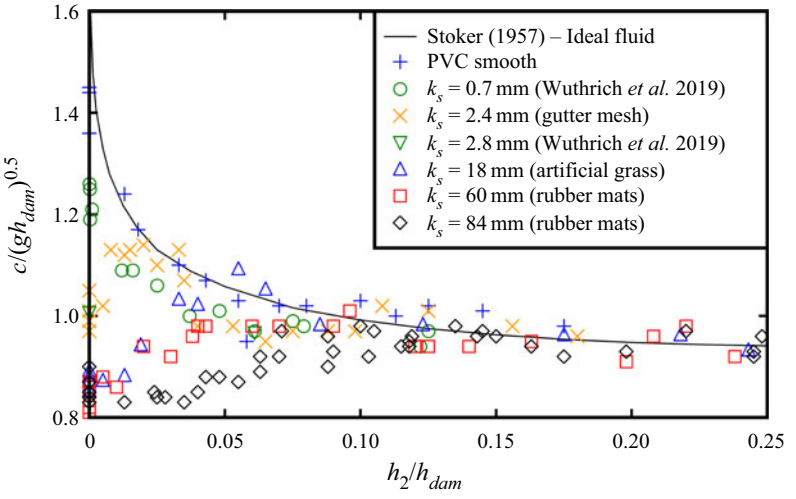

Figure 6. Quasi-steady tip propagation speeds for dam-break waves ($h_{dam} = 0.4$ m) on horizontal beds with different roughness k_s. Experimental data are compared with Stoker (1957).

with findings in figure 2 for the celerity. This confirms the validity of Stoker's paradigm that breaking bores reach a quasi-steady state during their propagation, both on dry and on wet beds.

4.1. *Comparison of real fluid data with Stoker's ideal fluid model*

The theoretical, steady propagation speeds obtained numerically from Stoker's model in (3.1) are compared with experimental data in figure 6. Good agreement is observed for the smooth PVC bed. The fact that these experimental celerities, observed within $10 < x/h_{dam} < 17.5$, converge to Stoker's model as the tailwater depth h_2 becomes greater than $0.5k_s$ (see figure 7 for details) encourages the strategy of using Stoker's model as a starting point for more general models of dam-break tip propagation on horizontal beds.

For relatively smooth beds ($k_s/h_{dam} < 0.002$), c decreases monotonically with increasing h_2 for $0 < h_2/h_{dam} < 0.35$, in analogy with Stoker's smooth bed solution. The three roughest beds tested in the present study ($k_s/h_{dam} > 0.045$) start, for a dry bed, with a tip quasi-steady propagation speed below Stoker's minimum value ($\sim 0.94\sqrt{gh_{dam}}$). Figure 6 shows that a bit of tailwater tends to promote the propagation speed compared with a dry bed such that c initially increases with h_2 and there is a local maximum of c for tailwater depths of the order of $0.5k_s$. The new experiments include only one dam height ($h_{dam} = 0.40$ m), however, the data from Wüthrich, Pfister & Schleiss (2019) with $k_s = 0.7$ and 2.8 mm include different dam heights $0.40\text{ m} < h_{dam} < 0.82$ m, showing the same trend in figures 6 and 7, thus adding credibility to the scaling applied herein.

5. Effect of friction for propagation onto dry horizontal beds

Observations of the quasi-steady speeds of dam-break tips propagating onto dry beds indicate that the retarding effects of roughness k_s and viscosity ν are similar to the effect of tailwater depth h_2, as long as the relevant relative 'friction lengths' k_s/h_{dam} and $\nu/\sqrt{gh_{dam}^3}$ are small, as shown in figure 8. That is, in the range $1 < c/\sqrt{gh_{dam}} < 1.5$, the curve

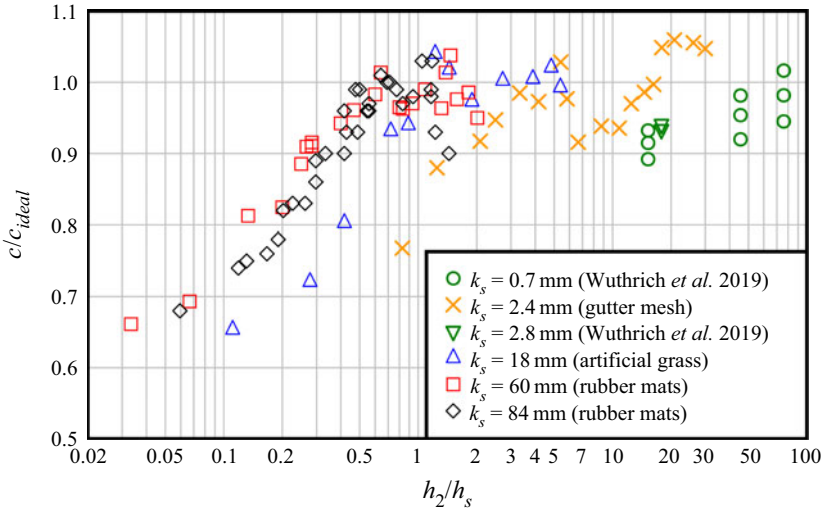

Figure 7. Quasi-steady tip propagation speed c for dam-break waves ($h_{dam} = 0.4$ m) on rough beds. Note that c reaches Stoker's ideal value for $h_2/k_s > 0.5$; c_{ideal} is computed using (3.1).

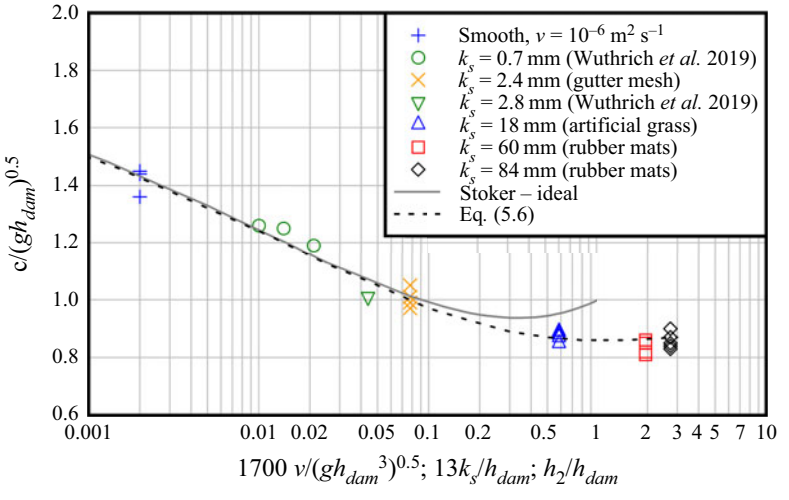

Figure 8. Stoker's $F(h_2/h_{dam})$ for ideal fluids works for moderately rough beds when applied as $F(13k_s/h_{dam})$ and for smooth beds when applied as $F(1700\nu/(gh_{dam}{}^3)^{0.5}$.

representing Stoker's ideal fluids theory and data from real fluids (water) on dry beds show very similar trends when the relevant relative length ratios are used as abscissa.

5.1. *Rough beds*

The data trends in figure 8 suggest that Stoker's theory for $c_{ideal}/\sqrt{gh_{dam}} = F(h_2/h_{dam})$ can be adopted for roughness effects on dry beds in the form $c_k/\sqrt{gh_{dam}} = F(\gamma_k(k_s/h_{dam}))$ with the 'roughness multiplier' $\gamma_k \approx 13$ for $k_s/h_{dam} < 0.01$. Hence, in close similarity to

Stoker's expression in (3.2), the rough bed data in figure 8 support the formula

$$\frac{c_k}{\sqrt{gh_{dam}}} = 2 - 3.36\left(13\frac{k_s}{h_{dam}}\right)^{1/4} + 3.54\left(13\frac{k_s}{h_{dam}}\right)^{1/2} + 1.14\left(13\frac{k_s}{h_{dam}}\right)^{3/4}, \quad (5.1)$$

for propagation onto dry, rough beds with moderate roughness: $k_s/h_{dam} < 0.01$.

The similarity of the retarding effect of a small k_s in (5.1) to that of a small h_2 expressed by (3.2) may be understood through the momentum equation for a steady dam-break tip with depth h_1 behind the 'shock' propagating with celerity c on a still tailwater depth h_2

$$\frac{1}{2}\rho g h_1^2 + \rho\int_{bed}^{surface}[u(x_1,z)-c]^2\,\mathrm{d}z = \frac{1}{2}\rho g h_2^2 + \rho c^2 h_2 + F_\tau, \quad (5.2)$$

where the unit friction force $F_\tau(x_1) = \int_{x_1}^{x_{tip}} \tau_{bed}\,\mathrm{d}x$ gives the cumulative effect of friction, truncated at a position x_1 behind the shock, where the bed shear stress becomes small and the depth is still quasi-steady, e.g. $t = 9$ s in figure 5(*a*).

Expecting that the friction (unit) force F_τ scales on ρc^2 and expressing it in terms of

$$L_\tau = \frac{F_\tau}{\rho c^2} = \frac{1}{\rho c^2}\int_{x_1}^{x_{tip}} \tau_{bed}\,\mathrm{d}x, \quad (5.3)$$

the momentum equation becomes

$$\frac{1}{2}\rho g h_1^2 + \rho h_1\left\{\left(c\frac{h_2}{h_1}\right)^2 + \mathrm{Var}[u_1(z)]\right\} = \frac{1}{2}\rho g h_2^2 + \rho c^2(h_2 + L_\tau), \quad (5.4)$$

where the last term shows the analogy between the influences of the friction related length L_τ and a small h_2. For greater tailwater depths, the h_2^2 term becomes dominant so that the influences of k_s and h_2 are no longer analogous. The 'exchange rate' between roughness and tailwater depth is indicated by the roughness multiplier $\gamma_k \approx 13$, which brings Stoker's theory in (3.2) $c_{ideal}/\sqrt{gh_{dam}} = F(h_2/h_{dam})$ in the form $c_k/\sqrt{gh_{dam}} = F(\gamma_k(k_s/h_{dam}))$ into agreement with the rough bed data in figure 8. That is, 1 mm of (dry) roughness has the same retarding effect as 13 mm of tailwater depth, or in terms of (5.4)

$$L_\tau \approx 13k_s, \quad \text{for } \frac{k_s}{h_{dam}} < 0.01. \quad (5.5)$$

For rougher beds, the effect of roughness is no longer analogous to that of the tailwater. Greater roughness has a stronger retarding effect than correspondingly deeper tailwater, a trend which is mimicked by the dashed curve in figure 8 given by

$$\frac{c_k}{\sqrt{gh_{dam}}} = 2 - 3.4\left(13\frac{k_s}{h_{dam}}\right)^{1/4} + 3.5\left(13\frac{k_s}{h_{dam}}\right)^{1/2} - 1.5\left(13\frac{k_s}{h_{dam}}\right)^{3/4} + 0.12\left(13\frac{k_s}{h_{dam}}\right), \quad (5.6)$$

where the coefficient to $(k_s/h_{dam})^{5/4}$ is zero, while Stoker's value is +0.407, giving the upward swing in his theory for $h_2/h_{dam} > 0.3$.

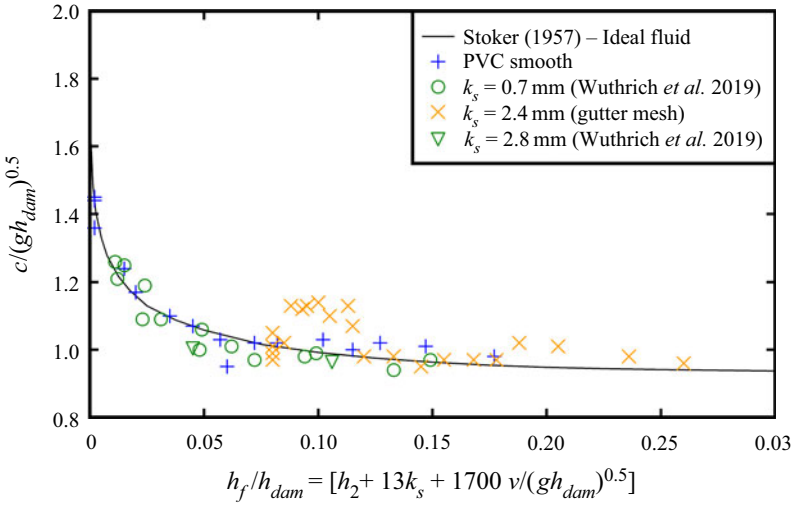

Figure 9. Combined effect of tailwater depth, viscosity and bed roughness on the tip propagation speed c.

5.2. *Smooth beds*

Similarly, the single set of (dry) smooth bed data in figure 8 supports the viscous formula

$$\frac{c_v}{\sqrt{gh_{dam}}} = 2 - 3.5\left(1700\frac{\nu/\sqrt{gh_{dam}}}{h_{dam}}\right)^{1/4} + 4\left(1700\frac{\nu/\sqrt{gh_{dam}}}{h_{dam}}\right)^{1/2} - 1.5\left(1700\frac{\nu/\sqrt{gh_{dam}}}{h_{dam}}\right)^{3/4}, \tag{5.7}$$

i.e. approximately Stoker's theory in (3.2) with the tailwater depth h_2 replaced by the viscous length $1700\nu/\sqrt{gh_{dam}}$.

5.3. *Combined small friction effects*

The fact that the small resistance contributions h_2, $13k_s$ and $1700\nu/\sqrt{gh_{dam}}$ have similar effects on c might suggest that suitably small terms of these forms act additively as in

$$\frac{c}{\sqrt{gh_{dam}}} = F\left(\frac{h_f}{h_{dam}}\right) = F\left(\frac{h_2 + 13k_s + 1700\nu/\sqrt{gh_{dam}}}{h_{dam}}\right). \tag{5.8}$$

The data in figure 9 show that this hypothesis works well for the viscosity dominated case of the smooth PVC data from the present study and for the data from Wüthrich *et al.* (2019). However, present data with $k_s = 2.4$ mm (gutter mesh) deviate for wet beds with $0.08 < h_f/h_{dam} < 0.12$, corresponding to $1 < h_2/k_s < 10$, where the tailwater acts as a lubricant. Outside this range, Stoker's theory with h_2 replaced by h_f shows good agreement.

6. Discussion

The initial stages of the dam-break wave propagation are difficult to model because the flow is non-hydrostatic and usually includes wave breaking (Stansby *et al.* 1998). It is also likely that even very small differences in the dam-opening process will generate big

differences in the shape of the initial breaking waves. However, Stoker (1957) and the present study show that the propagation of a dam-break tip can be considered quasi-steady beyond some distance from the dam position, if a finite amount of resistance is provided by the tailwater h_2, by the bed shear stress due to viscosity ν and/or by the roughness k_s. However, it is acknowledged that the viscosity was not systematically tested in the present study. Thus, application of the results and planning of further investigations call for more detailed information about the effect of viscosity on the length scale at which the tip propagation approaches a steady state (figure 2). To this end, the present study includes two experiments with detailed information about the settling down of the tip propagation. This led to length scales $L_x \approx 1.2$ m for rubber mats ($k_s = 84$ mm) and $L_x \approx 2.5$ m for a gutter mesh ($k_s = 2.4$ mm), corresponding to curve fits of the form $c(x) \approx c_{steady} + [c(0) - c_{steady}]e^{-x/L_x}$. Ritter's ideal fluid solution represents the resistance free limit $h_2, k_s, \nu \to 0$ and, in the sense that the depth at a given distance from the tip never becomes steady, it suggests $L_x \to \infty$ for the ideal fluid scenario. Together with this frictionless limit, the two tests suggest the tentative relation $L_x \approx 2.1 h_{dam}^{6/5} k_s^{-1/5}$. However, further experiments with real fluids and/or a numerical model are needed to resolve the dependence of L_x on the tailwater depth over a smooth bed.

One of the important new findings of the present study is that a small amount of tailwater, $h_2 < 0.5k_s$, acts as a lubricant in the sense that the tip propagates faster when the roughness elements are partly covered by water. However, the presently available data hint that this effect may be quite variable between beds with the same equivalent roughness, but different shapes. For instance, this lubrication effect is not observed for the data from Wüthrich *et al.* (2019) in figure 9, while it is quite prominent and consistent for the data with $k_s = 2.4$ mm from the present study. This might be attributed to the fact that Wüthrich *et al.* (2019) used an artificial rug with $k_s = 2.8$ mm, while herein $k_s = 2.4$ mm was obtained with a gutter mesh with 5 mm openings and 1 mm bar diameter. A useful reminder perhaps that, although different roughness geometries may show the same equivalent roughness in steady uniform flows, they may have very different effects on other kinds of flow, e.g. oscillatory flows or highly non-uniform flows under dam-break tips. The choices of different roughness geometries in the present study, including artificial grass, was partly motivated by this non-universality of k_s across different roughness geometries, partly by the fact that dam-break waves and tsunami run-ups often propagate over vegetation or granular beds.

A longer term aspiration of the present study is the development of suitable models for the boundary layer flow and sediment transport in the broader class of dam-break-like flows, including tsunamis and wind wave run-ups. Similarities would concern the very fast initial development of the bed shear on time scales of the order of 0.1 s (figure 5), well separated from the time scale of gravity-governed flows with depth $h \approx 1$ m on slopes $\beta \approx 0.1$, which is $h/\sqrt{\beta g} \approx 1$ s. Dam-break flows are expected to differ from steady uniform flows with respect to boundary layer scaling because they are both unsteady and non-uniform in the bed frame of reference. Perhaps useful analogies can be found with boundary layers downstream of the edge of a thin plate in steady uniform flow $u = u_\infty f(z, x, \nu, k_s)$, if the pressure gradient is neglected. However, while flows along semi-infinite, thin plates may be reasonably modelled as unidirectional (i.e. horizontal velocities only), the downwards flows towards the bed at the dam-break tip may need to be considered in order to model the large bed shear stresses and the corresponding sediment entrainment capacity at dam-break tips, as suggested by Nielsen (2018).

7. Conclusion

The front propagation speeds of dam-break waves in the range $10 < x/h_{dam} < 17.5$ were shown to be steady enough that comparisons with Stoker's (1957) steady model for smooth beds gave useful, quantitative indications of the retarding effect of dry bed friction. This also yielded indications on the interplay of the initial tailwater depth with bed roughness and/or viscosity in slowing down the dam-break tip propagation.

For moderate resistance, $13(k_s/h_{dam})$, $1700(\nu/\sqrt{gh_{dam}})/h_{dam} < 0.1$, the dry bed data in figure 8 can be represented by Stoker's ideal fluids function F corresponding to $c/\sqrt{gh_{dam}} = F(h_2/h_{dam})$ in the forms $c/\sqrt{gh_{dam}} = F(13k_s/h_{dam})$ for dry rough beds, and $c/\sqrt{gh_{dam}} = F(1700\nu/\sqrt{gh_{dam}})$ for smooth beds. Hence, for such modest flow resistance, $k_s = 1$ mm of roughness is equivalent to $h_2 = 13$ mm of tailwater and 1 μm of viscous length $\nu/\sqrt{gh_{dam}}$ is equivalent to 1700 μm of tailwater. For such relatively small h_2, k_s and $\nu/\sqrt{gh_{dam}}$ the resistance effects are additive, as expressed by (5.8) and shown in figure 9.

For fairly rough beds $k_s/h_{dam} > 0.01$, the effects of roughness are no longer analogous to those of tailwater. Thus, the data in figure 8 show that bore propagation is slower than Stoker's minimum value $0.94\sqrt{gh_{dam}}$ when these rough beds are dry. An addition of a small amount of tailwater ($h_2 \ll k_s$) initially acts as lubrication, and the observed increases of $c/\sqrt{gh_{dam}}$ amount to ∼20 % for the presently available experimental data, as detailed in figure 6.

The detailed effects of larger h_2/h_{dam}, k_s/h_{dam} or combined effects in $c = c(h_{dam}, h_2, k_s)$ are indicated qualitatively in figure 6 and provide interesting challenges for future and more detailed investigations towards a complete description of the flow structure, bed shear stresses and sediment transport near the tips of dam-break waves, tsunamis and wave run-ups.

Acknowledgements. The authors would like to thank Professor P. Perrochet and Professor A. Hogg for assistance with deriving the MacLaurin series for $c = c(h_2/h_{dam})$ according to Stoker's (1957) model. We would also like to thank Professor T. Baldock (The University of Queensland) for loaning his shear plate.

Funding. The financial support of The University of Queensland, School of Civil Engineering, and of the Swiss National Science Foundation (Grant P2ELP2_181794, D.W.) is acknowledged.

Declaration of interests. The authors report no conflict of interest.

Author ORCIDs.
Davide Wüthrich https://orcid.org/0000-0003-1974-3560;
Shaotong Zhang https://orcid.org/0000-0002-2806-2989.

References

Barnes, M.P. & Baldock, T.E. 2019 A Lagrangian model for boundary layer growth and bed shear stress in the swash zone. *Coastal Engineering* **57**, 385–396.

Chanson, H. 2009 Application of the method of characteristics to the dam break wave problem. *Journal of Hydraulic Research* **47** (1), 41–49.

Dressler, R.F. 1952 Hydraulic resistance effect upon the Dam–Break functions. *Journal of Research of the National Bureau Standards* **49** (3), 217–225.

Dressler, R.F. 1954 Comparison of theories and experiments for the hydraulic dam-break wave. *International Association Scientific Hydrology* **3** (38), 319–328.

Feynman, R., Leighton, R. & Sands, M. 1964 *Lecture 51 (shock waves)*. Feynman Lectures on Physics. Addison–Wesley.

Lauber, G. & Hager, W. 1998 Experiments to dam-break wave: horizontal channel. *Journal of Hydraulic Research* **36**, 291–307.

Nielsen, P. 2018 Bed shear stress, surface shape and velocity field near the tips of dam-breaks, tsunami and wave runup. *Coastal Engineering* **138**, 126–131.

NIELSEN, P. 2019 Bed shear stress, surface shape and velocity field near the tips of dam-breaks, tsunami and wave runup, Reply by P Nielsen. *Coastal Engineering* **152**, 103513.

PRITCHARD, D. & HOGG, A.J. 2002 Sediment transport under dam-break flow. *J. Fluid Mech.* **473**, 265–274.

RITTER, A. 1892 Die Fortpflanzung der Wasserwellen. *Zeitschrift Verein Deutscher Ingenieure* **36**, 947–954.

SCHOKLITSCH, A. 1917 Uber Dambruchwellen. *Kaiserliche Akademie der Wissenschaften, Wien, Mathematische-Naturwissenschaftliche Klasse* **IIA**, 1489–1514.

STANSBY, P., CHEGINI, A. & BARNES, T. 1998 The initial stages of dam-break flow. *J. Fluid Mech.* **374**, 407–424.

STOKER, J.J. 1957 *Water Waves*. Interscience.

WHITHAM, G. 1955 The effects of hydraulic resistance in the dam-break problem. *Proc Roy Soc London A* **227**, 399–407.

WÜTHRICH, D., PFISTER, M. & SCHLEISS, A.J. 2019 Effect of bed roughness on tsunami-like waves and induced loads on buildings. *Coastal Engineering* **152**, 103508.

XU, B., ZHANG, S., NIELSEN, P. & WÜTHRICH, D. 2021 Measurements of bed shear stresses near the tip of dam-break waves on a rough bed. *Exp. Fluids* **62**, 49.